JACS
JOURNAL OF THE AMERICAN CHEMICAL SOCIETY
Article
pubs.acs.org/JACS

Nonlinear Active Materials: An Illustration of Controllable Phase Matchability

Hongcheng Lu,[†,‡] Romain Gautier,[‡] Martin D. Donakowski,[‡] T.Thao Tran,[§] Bryce W. Edwards,[∥] Juan C. Nino,[∥] P. Shiv Halasyamani,[§] Zhengtang Liu,[†] and Kenneth R. Poeppelmeier*[,‡]

[†]State Key Laboratory of Solidification Processing, School of Materials Science and Engineering, Northwestern Polytechnical University, 127 Youyixilu Road, Xi'an 710072, China

[‡]Department of Chemistry, Northwestern University, 2145 Sheridan Road, Evanston, Illinois 60208, United States

[§]Department of Chemistry, University of Houston, Houston, Texas 77204, United States

[∥]Department of Materials Science and Engineering, University of Florida, Gainesville, Florida 32611, United States

Supporting Information

ABSTRACT: For a crystal to exhibit nonlinear optical (NLO) activity such as second-harmonic generation (SHG), it must belong to a noncentrosymmetric (NCS) space group. Moreover, for these nonlinear optical (NLO) materials to be suitable for practical uses, the synthesized crystals should be phase-matchable (PM). Previous synthetic research into SHG-active crystals has centered on (i) how to create NCS compounds and/or (ii) how to obtain NCS compounds with high SHG efficiencies. With these tactics, one can synthesize a material with a high SHG efficiency, but the material could be unusable if the material was nonphase-matchable (non-PM). To probe the origin of phase matchability of NCS structures, we present two new chemically similar hybrid compounds within one composition space: **(I)** $[Hdpa]_2NbOF_5{\cdot}2H_2O$ and **(II)** $HdpaNbOF_4$ (dpa = 2,2′-dipyridylamine). Both compounds are NCS and chemically similar, but **(I)** is non-PM while **(II)** is PM. Our results indicate—consistent with organic crystallography—the arrangement of the organic molecule within hybrid materials dictates whether the material is PM or non-PM.

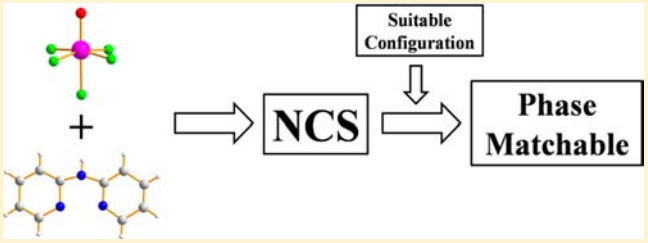

INTRODUCTION

Noncentrosymmetric (NCS) materials have been synthesized with early transition metal (ETM) octahedra and/or acentric organic molecules owing to the ability by which these basic-building units (BBUs) arrange into NCS configurations. Crystalline materials for second-order nonlinear optical (NLO) applications such as efficient second harmonic generation (SHG) activity require not only significant molecular hyperpolarizabilities but also NCS crystal packing.[1] When a material is NCS, it can have properties of piezoelectricity, ferroelectricity, and NLO activity.[2−5] Inorganic ETM oxides (e.g., $LiNbO_3$, $KTiPO_4$, and $BaTiO_3$, etc.) have been the premiere NLO-active materials. Their high efficiencies led to an investigation of how to construct crystals with greater efficiencies. Chen's anionic group theory stipulates that materials of distorted polar polyhedra can lead to high SHG efficiencies when the individual polar moments of the polyhedra align within the bulk.[6] Organic materials have been examined for use as NLO-active materials owing to large hyperpolarizability (β) values, ultrafast response times and architectural flexibility.[7,8] Conjugated molecules generally have larger hyperpolarizabilities owing to the extent of charge transfer (CT) and intermolecular interactions that can occur with delocalized π electrons.[8,9]

For an SHG-active material to be optically useful with ease and high efficiency, the material must be phase matchable (PM); for a non-PM material, the SHG efficiency decreases as the material's size increases in certain size ranges. The phase-matching technique is often used in both uniaxial and biaxial acentric crystals for SHG of light waves by mixing two strong collinear waves at the fundamental frequency to increase the SHG efficiency.[10−13] Phase matching of SHG is traditionally achieved by utilizing birefringent and dispersive properties of the crystal and is extremely sensitive to the refractive index. In specific directions of the crystal the refractive index of the harmonic wave is exactly the same as the refractive index of the fundamental wave, and the two waves travel through the crystal with exactly the same velocity; this results in phase matching in a crystal. However, there are crystals in which phase matching is not possible in any direction, for example, quartz.[12,14] NCS materials are typically synthesized first and then routinely measured experimentally to find phase matching conditions or to see if the specific directions for phase matching exist;[12,13,15,16] however, the relationship between phase matchability and crystal structure of NCS materials has been decidedly less discussed. Zyss and Oudar established relation-

Received: May 20, 2013
Published: July 18, 2013

   dx.doi.org/10.1021/ja4050604 | J. Am. Chem. Soc. 2013, 135, 11942−11950

ships between microscopic and macroscopic nonlinearities of molecular crystals and reported the optimal orientation of molecules within crystals for bulk phase matching;[17] To the best of our knowledge, the optimal phase-matching orientations of only a few molecules in their crystal structures have been individually reported (e.g., 2-(*N*-prolinol)-5-nitropyridine (PNP), *N*,*N*′-bis-(*p*-nitrophenyl)methanediamine (*p*-NMDA), and 3,5-dinitro-2-[[(*R*)-(−)-1-phenylethyl]amino]-pyridine).[18−20] To analyze the origin of phase matchability of NCS materials, this study presents an examination of the relationship between phase matchability and crystal structure of NCS materials, wherein two chemically similar SHG-active compounds are found in one composition space in which one is PM and one is non-PM. Two acentric basic-building units (BBUs) consisting of an acentric molecule, 2,2′-dipyridylamine (dpa), and a distorted ETM octahedron of a niobium cation resulted in two new NCS structures that are in the composition space of $NbO_{2.5}$/dpa/HF: compounds (**I**), $[Hdpa]_2NbOF_5{\cdot}2H_2O$, and (**II**), $HdpaNbOF_4$. Both compounds are SHG active: (**I**) and (**II**) belong to NCS space groups *P*1 and *Cc*, respectively. Despite their chemical similarity, non-PM compound (**I**) and PM compound (**II**) are synthetically controlled by modification of reactant ratios. We present a comparison of the two chemically similar NCS materials to rationalize the PM character of the hybrid material and the implications of this on design attempts to synthesize PM SHG-active materials.

EXPERIMENTAL SECTION

Caution. *Hydrofluoric acid is toxic and corrosive!* It must be handled with *extreme caution* and the appropriate protective gear.[21−23]

Materials. Niobium oxide (Nb_2O_5, 99.9%, Alfa Aesar), 2,2′-dipyridylamine ($C_{10}H_9N_3$, 99%, Aldrich) and aqueous hydrofluoric acid (48% HF by weight, Aldrich) were used as received.

Syntheses. Compound (**I**) was synthesized by adding 0.1000 g (3.76×10^{-4} mol) of Nb_2O_5, 0.4000 g (2.34×10^{-3} mol) of 2,2′-dipyridylamine, and 0.80 mL (2.21×10^{-2} mol) of 48% aqueous HF to a Teflon pouch;[24] compound (**II**) was synthesized by adding 0.2000 g (7.52×10^{-4} mol) of Nb_2O_5, 0.4000 g (2.34×10^{-3} mol) of 2,2′-dipyridylamine, and 0.80 mL (2.21×10^{-2} mol) of 48% aqueous HF to a Teflon pouch. The pouches were then sealed with an impulse sealer, placed into a 125 mL Parr autoclave with a backfill of 45 mL of deionized water, quickly heated to 200 °C, held at this temperature for 24 h, and cooled to ambient conditions at 0.1 °C/min. The colorless single crystals of (**I**) and colorless single crystals of (**II**) were recovered in air after vacuum filtration. The yields of (**I**) and (**II**) were 87.7% and 98.3% (based on Nb_2O_5), respectively.

Crystallographic Determination. Single-crystal X-ray diffraction data were obtained on a Bruker-APEX II CCD diffractometer with monochromatic Mo Kα radiation (λ = 0.71069 Å) at 100 K for (**I**) and with monochromatic Cu Kα radiation (λ = 1.54178 Å) at 293 K for (**II**). The crystal-to-detector distance was 60 mm, and data integrations were made using SAINT-V7.23A.[25] Multiscan absorption corrections were applied to the data with SADABS.[26] The structures were determined by direct methods, completed by Fourier difference syntheses with SIR97[27] for (**I**) and SIR2004[28] for (**II**), and refined using SHELXL-97.[29] No higher symmetry or unit cells were found by examination with PLATON.[30] Hydrogen atoms of dpa molecules were included in the refinement model as riding atoms in idealized positions (C−*H* = 0.93 Å, N−*H* = 0.86 Å, and U_{iso}(H) = 1.5U_{eq}(C,N)). Crystallographic data are reported in Table 1.

FTIR Spectroscopy. The FT-IR spectra of both compounds were collected on a Bruker 37 Tensor FTIR equipped with an ATR germanium cell. A total of 256 scans were recorded from 600 to 4000 cm^{-1} at a 4 cm^{-1} resolution, and a background spectrum was subtracted.

Table 1. Crystal Data, Structure Solutions and Refinements for $[Hdpa]_2NbOF_5{\cdot}2H_2O$, (I), and $HdpaNbOF_4$, (II)

formula	$[Hdpa]_2NbOF_5{\cdot}2H_2O$	$HdpaNbOF_4$
formula weight ($g{\cdot}mol^{-1}$)	584.36	357.12
temperature (K)	100(2)	293(2)
crystal system	triclinic	monoclinic
space group	*P*1	*Cc*
a (Å)	7.2697(4)	20.2084(5)
b (Å)	9.0944(5)	3.98043(9)
c (Å)	9.7580(5)	15.7991(4)
α (deg)	63.382(2)	90
β (deg)	73.810(2)	109.3866(13)
γ (deg)	80.398(2)	90
V (Å^3)	553.23(5)	1198.90(5)
Z	1	4
maximum 2θ (°)	30.7	67.4
λ(Mo/Cu) Kα (Å)	0.71069	1.54178
$\rho_{calc.}$ ($g{\cdot}cm^{-3}$)	1.754	1.979
R_{int}	0.024	0.017
R_1	0.035	0.022
wR_2	0.093	0.06
goodness-of-fit	1.08	1.11
dimension (mm)	0.30 × 0.21 × 0.19	0.18 × 0.10 × 0.04

Thermogravimetric Analysis (TGA). The TGA measurements for both compounds were performed on a TGA Q50 with a standard furnace under an argon atmosphere with a heating rate of 1 °C/min from ambient temperature to 900 °C. The materials were held at this temperature for 5 h and then cooled to room temperature at a rate of 1 °C/min.

Second Harmonic Generation Measurements. Powder SHG measurements were performed on a modified Kurtz nonlinear optical (NLO) system using a pulsed Nd:YAG laser with a wavelength of 1064 nm.[31,32] A detailed description of the equipment and methodology has been published.[33] As the powder SHG efficiency has been shown to strongly depend on particle size,[32] (**I**) and (**II**) were ground and sieved into distinct particle size ranges (<20, 20−45, 45−63, 63−75, 75−90, >90 μm). Relevant comparisons with known SHG materials were made by grinding and sieving crystalline α-SiO_2 and $LiNbO_3$ into the same particle size ranges. No index matching fluid was used in any of the experiments.

Impedance Measurements. Impedance measurements were performed to determine if (**II**) exhibited piezoelectric resonance; we were unable to obtain large single crystals of (**I**) that were suitable for impedance measurements. A single crystal of (**II**) was painted with silver paste on opposing parallel flat facets and air-dried to form a parallel plate capacitor (metal insulator metal, MIM) with good electrical contacts. The piezoelectric resonance characteristics of the MIM were analyzed at room temperature using an Agilent 4294A precession impedance analyzer (PIA). The magnitude and the phase angle of the impedance were both collected from 40 kHz to 2 MHz. The resonance and antiresonance frequencies were obtained by fitting the peaks observed in the admittance and impedance plots to a Gaussian distribution. Owing to the irregular dimensions of the typical crystals, the effective coupling coefficient k^2_{eff} was calculated using eq 1

$$k^2_{eff} = \frac{f_n^2 - f_m^2}{f_n^2} \quad (1)$$

where f_n^2 is the resonance frequency and f_m^2 is the antiresonance frequency. This equation assumes a mechanical quality factor greater than 10^2. This is a reasonable assumption given the number of overtones and the suitable FWHM (~2 kHz, < 0.5%) of the main resonant peak.[34]

dx.doi.org/10.1021/ja4050604 | J. Am. Chem. Soc. 2013, 135, 11942−11950

RESULTS

The $NbO_{2.5}$/dpa/HF Composition Space. A composition space diagram analysis can directly compare the effects of different initial reactant concentrations on the composition or phases of the final products. We performed additional experiments with varied ratios of reagents in aqueous hydrofluoric acid to examine the composition space of $NbO_{2.5}$/dpa/HF which was placed by different mass ratios of the reactant metal oxides, 2,2′-dipyridylamine and HF as shown in Figure 1. Four distinct crystallization fields occur in this system. In region A, colorless single crystals of $[Hdpa]_2NbOF_5{\cdot}2H_2O$ (**I**) were observed. Colorless single crystals of $HdpaNbOF_4$ (**II**) were observed in region B. In region C, NbO_2F was formed, as determined by powder XRD (JCPDS card 47-1231); in region D, unreacted Nb_2O_5 (JCPDS card 27-1312) remained.

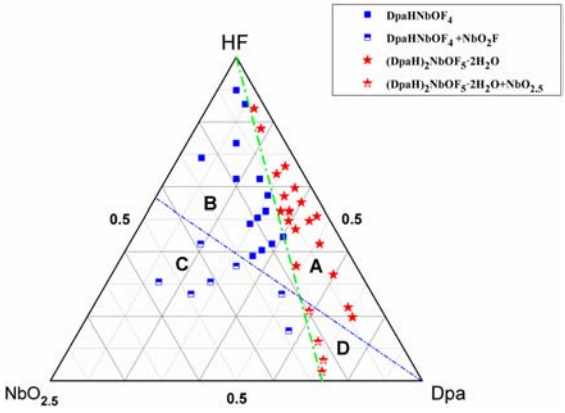

Figure 1. Composition space of the $NbO_{2.5}$, dpa, and HF system in mass ratios.

Structural Descriptions. Noncentrosymmetric structures of (**I**) and (**II**) both contain niobium oxide-fluoride anions and acentric $[Hdpa]^+$ cations.

The structure of (**I**) in the space group *P*1 contains disordered 0D BBUs of $[NbOF_5]^{2-}$, see Figure 2. The six Nb−F or Nb−F/O bond distances range from 1.907(3) Å to 1.940(3) Å (see Table 2). The niobium oxide-fluoride anion $[NbOF_5]^{2-}$ link via the $[Hdpa]^+$ cation through N−H$^+$···F hydrogen bonding (where N−H$^+$ is the bridging amine of $[Hdpa]^+$). Hydrogen bonding additionally occurs through O−H$^+$···F and N−H$^+$···O interactions, linking the water molecules to the $[NbOF_5]^{2-}$ cluster and dpa ligands (Figure 4a and Table 3). Two nitrogen and carbon atoms are disordered within aromatic rings owing to molecular rotation of the pyridine rings around the amine bridge.

Table 2. Selected Bond Lengths R_i for Compounds (I) and (II)

$[Hdpa]_2NbOF_5{\cdot}2H_2O$ (**I**)		$HdpaNbOF_4$ (**II**)	
bond	R_i, Å	bond	R_i, Å
Nb_1—F_6	1.907(3)	Nb_1—O_1	1.748(3)
Nb_1—F_5	1.918(3)	Nb_1—F_4	1.854(4)
Nb_1—F_1/O_1	1.920(3)	Nb_1—F_1	1.894(4)
Nb_1—F_4/O_4	1.930(3)	Nb_1—F_3	1.913(4)
Nb_1—F_2/O_2	1.932(4)	Nb_1—F_2	1.989(4)
Nb_1—O_3/F_3	1.940(3)	Nb_1—O_1	2.235(2)

The crystal structure of (**II**) in the space group *Cc* consists of infinite chains of an ordered 1D BBUs of $[NbOF_4]^-$ anions linked by shared vertice-oxygen atoms. The $[Hdpa]^+$ cations occupy the spaces between the chains, as shown in Figure 3. The $[NbOF_4]^-$ anions form in continuous and parallel chains along the *b* axis through an oxygen bridge. The anions show a strong distortion owing to the second-order Jahn−Teller effect.[35,36] As described by the glide plane along the *b* axis, the polar chains of $[NbOF_4]^-$ align in an antiparallel configuration. Each distorted niobium octahedron is composed of four equatorial Nb−F bonds and two bridging O−Nb−O bonds, one long Nb−O bond and one short Nb−O bond. The mean equatorial Nb−F bond distance is 1.913(4) Å, the short Nb═O bond length is 1.748(3) Å, and the long Nb−O bond is 2.235(2) Å (Table 2). These distances correspond with previously reported 1D chains of $[NbOF_4]^-$.[37,38] The planar $[Hdpa]^+$ molecules exist on two planes that are at an angle of

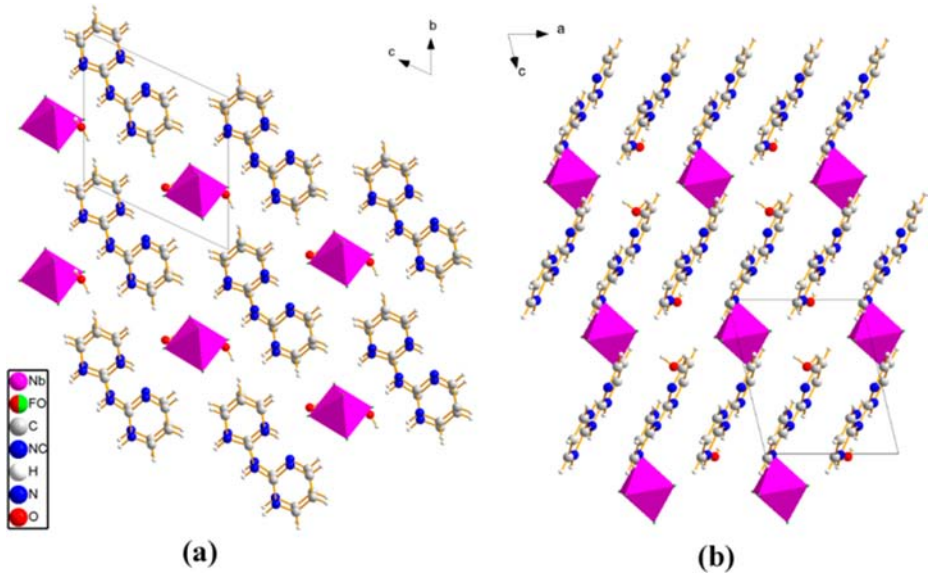

Figure 2. Perspective view of the structure of compound (**I**) (a) along axis *a*; (b) along axis *b*.

dx.doi.org/10.1021/ja4050604 | J. Am. Chem. Soc. 2013, 135, 11942−11950

Table 3. Hydrogen-Bonding Geometric Data (Å, deg) in Compounds (I) and (II)

$[Hdpa]_2NbOF_5{\cdot}2H_2O$ (I)			$HdpaNbOF_4$ (II)		
D−H···A	H···A (Å)	D−H···A (deg)	D−H···A	H···A (Å)	D−H···A (deg)
$N_4-H_{4N}...F_3/O_3$	1.80	165.0	$N_1-H_{1N}\cdots F_4$	1.97	158.3
$N_2-H_{2N}\cdots F_1/O_1$	2.53	129.3	$N_2-H_{2N}\cdots F_2$	2.85	132.5
$O_{2W}-H_{4W}\cdots F_2/O_2$	2.00	161.8			
$O_{1W}-H_{2W}\cdots F_2/O_2$	1.99	175.3			
$O_{1W}-H_{1W}\cdots F_4/O_4$	2.10	158.5			
$N_1-H_{1N}\cdots O_{2W}$	1.81	165.4			
$N_5-H_{5N}\cdots O_{1W}$	2.55	125.4			

62.7°; these planes are related by the glide plane of *C*. Hydrogen bonding occurs through N−H$^+$···F interactions, linking the lattice 2,2′-dipyridylamine molecules to the infinite $[NbOF_4]^-$ chain (Figure 4b and Table 3).

FTIR Spectroscopy. X-ray crystallography is unable to definitively distinguish an oxide from a fluoride ligand owing to their similar polarizability and ionic radii.[39] To validate that the oxide-fluoride BBUs in (I) and (II) consist of 0D BBUs of $[NbOF_5]^{2-}$ and 1D BBUs of ordered $[NbOF_4]^-$, respectively, we employed FTIR spectroscopy to assign the niobium oxide-fluoride of (I) as $[NbOF_5]^{2-}$ and (II) as $[NbOF_4]^-$. The infrared spectrum of (I) (Figure 5a) shows a characteristic band for $[NbOF_5]^{2-}$ at ν_s(Nb═O) = 896 cm^{-1},[37,40,41] and the infrared spectrum of (II) (Figure 5b) show a strong broad characteristic band for $[NbOF_4]^-$ at ν_s(Nb−O−Nb) = 799 cm^{-1},[42,43] respectively. The strong ν_s(Nb═O) or ν_s(Nb−O−Nb) peaks show that Nb═O bonds are present in both structures. Characteristic absorptions at 3122, 1656, 1604, 1559, 1454, and 769 cm^{-1} are attributable to the 2,2′-dipyridylamine ligand.[44] The broad absorption around 3440 cm^{-1} for compound (I) is assigned to water molecules within the lattice structure.

Thermal Analysis. To further verify the structures and contents of (I) and (II), TGA was performed. The TGA curves of (I) and (II) show a weight loss of (I) (80.4%) that mainly corresponds to the loss of water and dpa molecules and a weight loss of (II) (69.6%) that mainly corresponds to dpa molecule, respectively (see the Supporting Information [SI], Figure S1). The calculated losses of (I) (81.3%) and (II) (69.5%) correspond to niobium monoxide (NbO). After heating (I) and (II) to 900 °C, a white polycrystalline sample remained. For both (I) and (II), the polycrystalline samples were identified as Nb_2O_5 by powder X-ray diffraction (JCPDS PDF No. 37-1468). We attribute the change from NbO to Nb_2O_5 to oxidation of NbO in air.

Second Harmonic Generation (SHG) Properties. Compounds (I) and (II) were examined with Kurtz−Perry SHG measurements to investigate their NLO properties. (I) and (II) both exhibit SHG efficiencies at an order of magnitude higher than that of α-SiO_2. The measurements indicate that (I) has an SHG efficiency ∼40 times that of α-SiO_2 and is not type 1 PM (non-PM) (Figure 6a). Compound (II) is type 1 PM with an SHG efficiency of ∼30 times that of α-SiO_2 (Figure 6b). The average NLO susceptibilities, d_{ijk}^{2w}, of (I) and (II) were calculated by eq 2 for non-PM materials and eq 3 for PM materials.[32,45,46]

$$\frac{I^{2w}(I)}{I^{2w}(SiO_2)} = \frac{\langle d(I)_{ijk}^{2w}\rangle^2}{0.3048} \quad (2)$$

$$\frac{I^{2w}(II)}{I^{2w}(LiNbO_3)} = \frac{\langle d(II)_{ijk}^{2w}\rangle^2}{\langle d(LiNbO_3)_{ijk}^{2w}\rangle^2} \quad (3)$$

In these formulas, $I^{2w}(\sigma)$ is the SHG intensity of (I) or (II), $I^{2w}(SiO_2)$ is the intensity of a standard of α-SiO_2, and $\langle d(LiNbO_3)_{ijk}^{2w}\rangle^2 = 7.98 \times 10^2$ pm^2/V^2.[47] The values of $I^{2w}(\sigma)$ and $I^{2w}(SiO_2)$ were measured at the same range of particle sizes of each compound. Equation 2 is suitable for non-PM compounds, and eq 3 is suitable for PM compounds. To calculate d_{ijk}^{2w} of compound (II), $I^{2w}(LiNbO_3)$ was substituted by $600 \times I^{2w}(SiO_2)$.[32,33] The average NLO susceptibilities d_{ijk}^{2w} of (I) and (II) are approximately 3.5 pm/V and 6.3 pm/V,

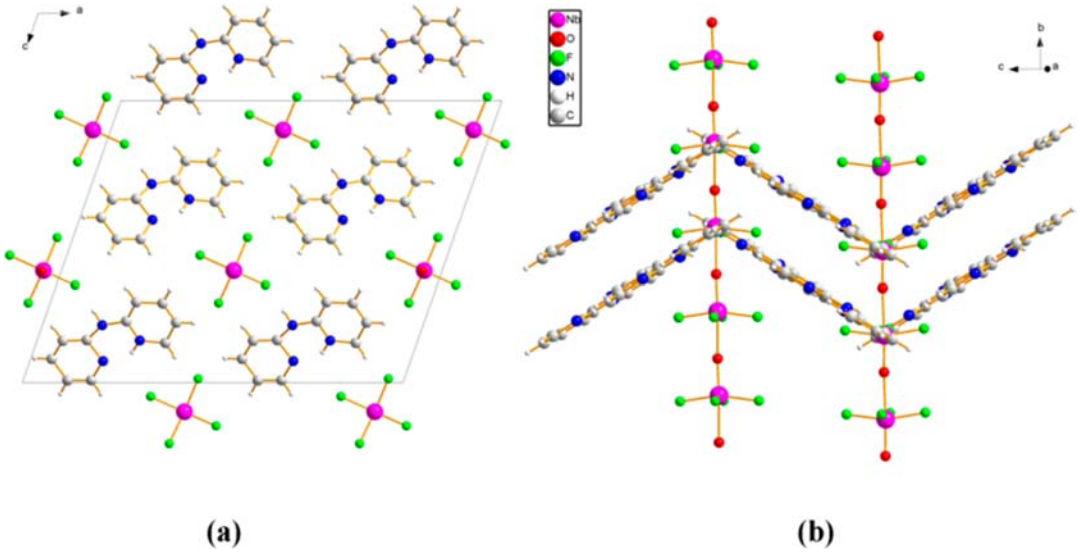

Figure 3. Perspective view of the structure of compound (II), (a) along axis *b*; (b) view of chains.

dx.doi.org/10.1021/ja4050604 | J. Am. Chem. Soc. 2013, 135, 11942−11950

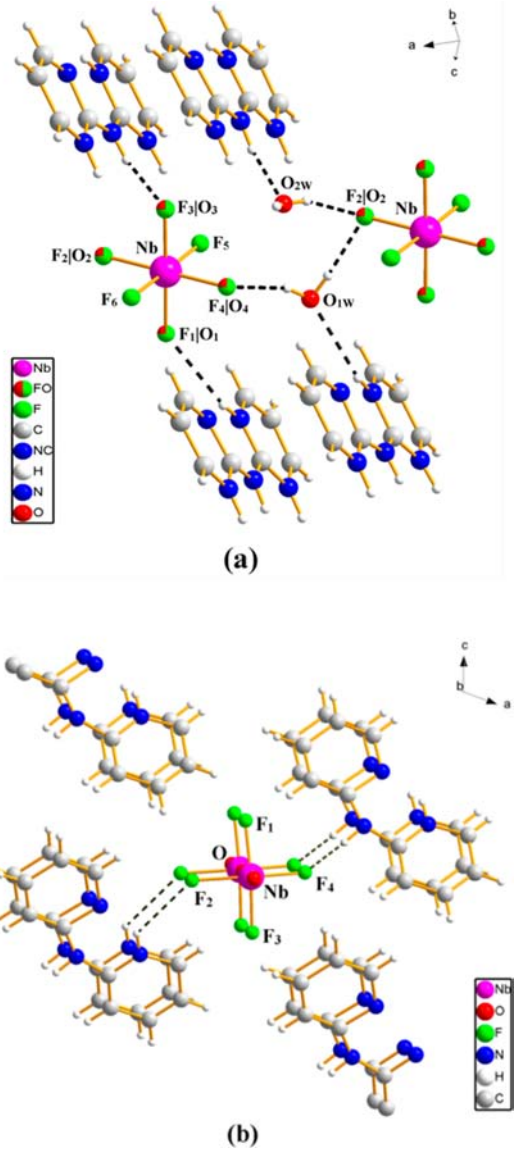

Figure 4. Hydrogen bonds to the oxide-fluoride ions of niobium complexes (a) in compound (**I**); (b) in compound (**II**).

respectively. As such, (**I**) and (**II**) respectively are included in the SHG categories C and B, as defined by Kurtz and Perry (Figure 6).[32]

Impedance Properties. As mentioned, we were unable to grow crystals of (**I**) with suitable size and quality for piezoelectric measurements; however, Figure S2 in SI shows that (**II**) exhibits piezoelectric resonant behavior (see SI). Several resonant peaks are present within a narrow frequency range, and several in-plane resonant modes are expected owing to imperfect crystal morphology. The k_{eff} was calculated with eq 1, and the results are shown in Table 4. These values are similar to those of the AT-cut of quartz crystals with $k_{26} = 0.088$[48] and $CuVOF_4(H_2O)_7$ with $k_{eff} = 0.093$ previously reported by our group.[49] It is important to note that a high k_{eff} is desirable for commercial applications involving handling of mechanical power; however, given the inherent low mechanical properties of these crystals, their use in electronic piezoelectric applications such as signal filters may be more appropriate.

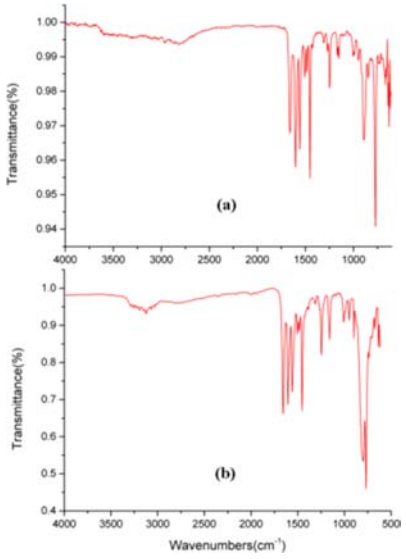

Figure 5. FTIR spectra of (a) compound (**I**) and (b) compound (**II**).

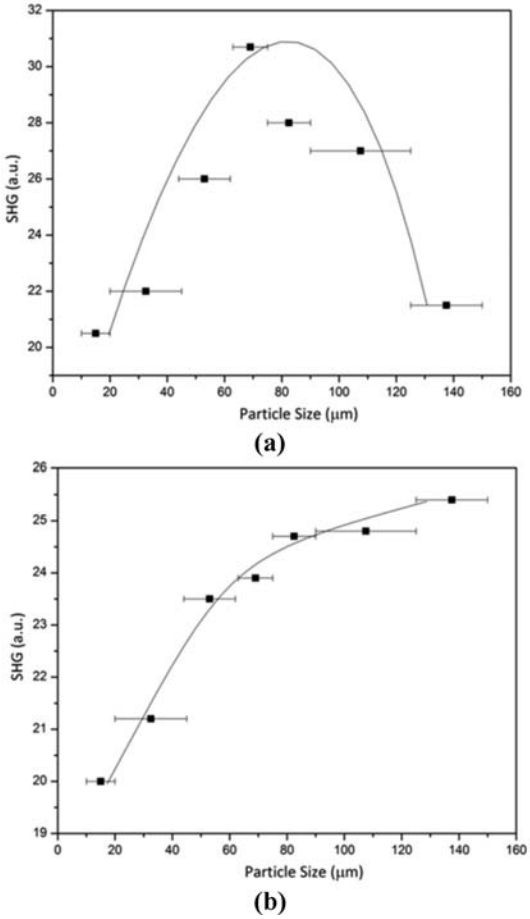

Figure 6. Phase matching curve and SHG intensities as a function of particle size. (a) Compound (**I**); (b) compound (**II**).

DISCUSSION

Formation of Anion $[NbOF_5]^{2-}$ or $[NbOF_4]^-$. In structures (**I**) and (**II**), $[NbOF_5]^{2-}$ or $[NbOF_4]^-$ anions are synthesized by use of different dpa:Nb ratios. Compound (**I**) is synthesized with a mole ratio of dpa:Nb greater than 2:1; compound (**II**) is synthesized with a dpa:Nb mole ratio less

dx.doi.org/10.1021/ja4050604 | J. Am. Chem. Soc. 2013, 135, 11942−11950

Table 4. Representative Piezoelectric Resonant and Antiresonant Frequencies for Compound (II) and the Corresponding Calculated Effective Electromechanical Coupling Coefficient

frequency range (kHz)	f_n (kHz)	f_m (Hz)	k^2_{eff} ($\times 10^{-3}$)	k_{eff}
407–415	413.0	411.5	6.978	0.084
975–990	985.3	983.3	4.095	0.064

than 2:1. This results in (**I**) having a dpa:Nb mole ratio of 2:1 and (**II**) having a dpa:Nb mole ratio of 1:1. The composition space diagram (see Figure 1) illustrates this trend: $[Hdpa]_2NbOF_5{\cdot}2H_2O$ (**I**) is synthesized only in region A. In region B where the dpa:Nb mol ratio is less than 2:1, $HdpaNbOF_4$ (**II**) dominates because there are insufficient $[Hdpa]^+$ cations to crystallize the 2:1 mol ratio of dpa:Nb in the structure of $[Hdpa]_2NbOF_5{\cdot}2H_2O$ (**I**). White polycrystalline samples were obtained with crystals at low HF concentration (mole ratio about HF:Nb ≤ 9:1) in regions C and D. In region C, NbO_2F was formed with crystals of $HdpaNbOF_4$ (**II**). In region D, unreacted Nb_2O_5 was observed with crystals of $[Hdpa]_2NbOF_5{\cdot}2H_2O$ (**I**). We note that crystals were easily grown in high yield even at low concentrations of the ETM (mole ratio HF:Nb = 176:1), and crystal quality became better with increasing Nb_2O_5 ratio in the reactants. This contrasts with composition space diagrams reported by Halasyamani et al.[24,40] and Norquist et al.[50] in which distinct regions exist without crystal formation at low ETM concentration.

In previous papers,[51−53] NMR has been used to identify the niobium anion species in solution as a function of the F:Nb mole ratio and/or fluoride concentration owing to anion exchange in solution. Ilyin et al.[51,54] reported that *trans*-$[NbOF_4{\cdot}H_2O]^-$ exists in solutions containing mole ratios of F:Nb ≤ 5. After basic hydrolysis by increasing alkalinity, the anion, $[NbOF_5]^{2-}$, forms. Kasamatsu et al.[52] and Monroy-Guzman et al.[53] reported that $[NbOF_4]^-$ is present at fluoride concentrations of 2.0×10^{-4} and 3.0×10^{-3} M, $[NbOF_5]^{2-}$ is the dominant species at $[F^-] = 8.9 \times 10^{-3}$–$1.9 \times 10^{-2}$ M, and $[NbF_6]^-$ and $[NbF_7]^{2-}$ are formed when $[F^-] > 11$ M. Throughout these concentrations, $[NbOF_5]^{2-}$ is present in varying quantities.[52]

In this study under hydrothermal conditions, the mole ratio of dpa:Nb appears to be the controlling factor in the crystal growth of $[Hdpa]_2NbOF_5{\cdot}2H_2O$ (**I**) versus $HdpaNbOF_4$ (**II**). The niobium oxide-fluoride anion $[NbOF_4]^-$ of (**II**) forms in a solution with a mole ratio of dpa:Nb < 2:1. The anion of (**I**), $[NbOF_5]^{2-}$ forms in a solution with a dpa:Nb molar ratio of 2:1. High dpa concentrations in solutions can provide a large $[Hdpa]^+$ cation concentration with the disassociation of HF to favor the formation of the $[NbOF_5]^{2-}$ anion with increasing alkalinity with a high fluoride concentration.

Structure and Hydrogen Bonding. Both compounds (**I**) and (**II**) consist of niobium oxide-fluoride anions and 2,2′-dipyridylamine cations where the fluoride anion hydrogen bonds to the acidic hydrogen of a dpa ligand (see Figure 2). We note that positioning of hydrogen atoms is difficult with X-ray diffraction and were placed in calculated positions. These positions do not take into account the bond length alterations caused upon hydrogen bonding[55] (corrections for hydrogen-bond geometry with fluoride ions has not been established). For the purposes of the structural discussion we included a tentative discussion of hydrogen-bond geometry based upon our best available option: calculated hydrogen atom positions. In $[Hdpa]_2NbOF_5{\cdot}2H_2O$ (**I**), a 0D BBU of $[NbOF_5]^{2-}$ is isolated in a hydrogen-bond network created by the two $[Hdpa]^+$ cations and two water molecules. In this niobium octahedron, niobium−ligand bond distances range from 1.907(3) Å to 1.940(3) Å (Table 2). The Nb═O bond in (**I**) has been confirmed by IR spectrum at ν_s(Nb═O) = 896 cm^{-1} (see Figure 5a). It was not possible to distinguish the oxide anions from the fluoride anions via X-ray diffraction. The similar bond distances indicate that the O^{2-}/F^- anions may be disordered among the six frequent positions. This has been previously observed in the disordered structure of $[C_9H_8NO]_2[NbOF_5]{\cdot}2H_2O$ in which niobium ion O^{2-}/F^- distances were found to range from 1.909(5) Å to 1.943(4) Å.[56] However, owing to no observation of strong hydrogen-bonding interactions to F_5 and F_6, disorder over four orientations is more likely in the structure of (**I**). F_5 and F_6 are fully ordered fluorides, and the remaining ions are disordered oxide-fluorides sites. Hydrogen bonding among $[Hdpa]^+$ cations, $[NbOF_5]^{2-}$ anions, and water molecules can affect the Nb−F bond distances.[57] The Nb−F_3/O_3 bond with the length of 1.940(3) Å is longer than the Nb−F_5/O_5, F_6/O_6 owing to a strong hydrogen bond ($H_{4N}{}^+\cdots F_3/O_3$= 1.80 Å) with the amine on $[Hdpa]^+$ cations (Figure 4a and Table 3). The Nb−F_2/O_2 bond with the length of 1.933(4) Å and the Nb−F_4/O_4 bond with the length of 1.929(3) Å, also longer than the Nb−F_5/O_5, F_6/O_6, form hydrogen bonds with water molecules through O_{1W}−$H_{2W}{}^+\cdots F_2/O_2$ ($H_{2W}{}^+\cdots F_2$ = 1.99 Å), O_{2W}-$H_{4W}{}^+\cdots F_2/O_2$ ($H_{4W}{}^+\cdots F_2$ = 2.00 Å) and O_{1W}-$H_{1W}{}^+\cdots F_4/O_4$ ($H_{1W}{}^+\cdots F_4$ = 2.10 Å) interactions, respectively. Hydrogen bonding also occurs through N_1−$H_{1N}{}^+\cdots O_{2W}$ ($H_{1N}{}^+\cdots O_{2W}$ = 1.81 Å) and N_5−$H_{5N}{}^+\cdots O_{1W}$ ($H_{5N}{}^+\cdots O_{1W}$ = 2.55 Å) interactions, linking water molecules to dpa ligand. Strong hydrogen bonds through N−$H^+\cdots$F($H^+\cdots F$ = 1.80 Å) and N−H$\cdots$O ($H^+\cdots O$ = 1.83 Å) also occurs in the similar ordered structure of $[H_2N(C_2H_4)_2NH_2][NbOF_5]$.[58] A similar structure with isolated $[NbOF_5]^{2-}$ has been reported by Buslaev et al.[59] in $N_2H_6NbOF_5{\cdot}H_2O$ in which the $[N_2H_6]^{2+}$ cation is replaced by $[Hdpa]_2{}^{2+}$ and water molecules in $[Hdpa]_2NbOF_5{\cdot}2H_2O$ (**I**) in this study.

In $HdpaNbOF_4$(**II**), infinite $[NbOF_4]^-$ chains are formed by sharing O vertices in the distorted $[NbO_{2/2}F_4]^-$ octahedra, where these intraoctahedra distortions align down the chain in a polar fashion. Neighboring chains face opposing directions which cancels their dipole moments. (Figure 3). Each niobium cation is in a distorted octahedral coordination geometry with two *trans*-O anions (Nb═O at 1.748(3) Å and Nb−O at 2.235(2) Å) and four equatorial F atoms within an Nb−F range of 1.854(4)−1.989(4) Å (Table 2). The niobium cation is shifted 0.244 Å from the equatorial plane toward the oxide ion. The shortest Nb−O bond with distance 1.748(3) Å in (**II**) is too short for a single bond and indicates a weak triple bond should be present, which causes a distortion of the Nb^{5+} cation in an octahedral environment owing to the second-order Jahn−Teller effect.[35,36] Compared to the corresponding bond in isolated ions like $[NbOF_5]^{2-}$, sharing of an oxide ion by two central niobium atoms in the structure with chains ($[NbOF_4]^-$) weakens the binary Nb═O bond. This decreases the frequency of Nb−O vibrations in IR spectra in the case of isolated oxide-fluoride complex ions.[43] The IR vibration of bridging the Nb−O−Nb bond in compound (**II**) is at ν_s(Nb−O−Nb) = 799 cm^{-1} (see Figure 5b). The frequency decreases as compared with ν_s(Nb═O) = 896 cm^{-1} in (**I**).[42,43,60] The Nb−F_2 bonds

dx.doi.org/10.1021/ja4050604 | J. Am. Chem. Soc. 2013, 135, 11942−11950

with the length of 1.989(4) Å, longer than the Nb−F_1, F_3, form hydrogen bonds with $[Hdpa]^+$ cation through N_2−$H_{2N}{}^+\cdots F_2$ interaction. The niobium oxide-fluoride anions $[NbOF_4]^-$ are also linked via the $[Hdpa]^+$ cations through another N_1−$H_{1N}{}^+\cdots F_4$ hydrogen bonding (Figure 4b and Table 3). A structure similar to that of $HdpaNbOF_4$ with infinite $[NbOF_4]^-$chains has been reported by Pakhomov et al.[61] in NH_4NbOF_4. Electrostatic interactions exist between the protonated $[Hdpa]^+$ cations and $[NbOF_5]^{2-}$ anions in (**I**), $[NbOF_4]^-$anions in (**II**), respectively. These hydrogen-bonding and electrostatic interactions stabilize the crystal structures of compounds (**I**) and (**II**).

It is interesting to note that the structure of (**II**), $HdpaNbOF_4$, exists in the monoclinic crystal system with a/b = 5.1, c/b = 4.0, and Z = 4. Many structures with infinite $[NbOF_4]^-$chains crystallize in the monoclinic or orthorhombic crystal systems with a/b and $c/b \geq 4$ (chain along b axis) and Z = 4. For example, a/b = 4.2, c/b = 5.1, and Z = 4 for $[Hphen][NbOF_4]\cdot H_2O$;[62] b/c = 5.6, a/c = 4.3, and Z = 4 for Cu(bpy) $NbOF_4\cdot 2H_2O$;[38] b/a = 4.4, c/a = 5.8, and Z = 4 for $Ag(bpy)NbOF_4\cdot 2H_2O$[38] (phen =1,10-phenanthroline). Infinite $[NbOF_4]^-$ chains within a hydrogen-bond network created directly with organic cations have been reported in the centrosymmetric (CS) structures of NH_4NbOF_4[61] and $[Hphen][NbOF_4]\cdot H_2O$[62] and in the NCS structure of (**II**) $HdpaNbOF_4$ in this study. The $[NbOF_5]^{2-}$ anion exists in the CS structures of $N_2H_6NbOF_5\cdot H_2O$,[59] $[C_9H_8NO]_2[NbOF_5]\cdot 2H_2O$,[56] $(C_5H_{12}NO_2)_2NbOF_5$,[63] $(C_3H_8NO_2)_2[NbOF_5]\cdot 2H_2O$,[64] $(C_2H_6NO_2)_2[NbOF_5]$,[64] $[H_2N(CH_4)_2NH_2][NbOF_5]$,[58] and the NCS structure of $[Hdpa]_2NbOF_5\cdot 2H_2O$ (**I**) in this study. Centrosymmetric structures of other metals with dpa molecules exist in $[H_2dpa]_2[V_2O_2F_8]$,[44] $HdpaPF_6\cdot H_2O$,[65] $[Hdpa]_2MnCl_4$,[66] and other dpa derivatives.[67−69] These CS structures are a result of antiparallel or other centric-type stacking of dpa molecules. To the best of our knowledge, no NCS structure has been previously formed by direct combination of acentric dpa molecules with other species.

Nonlinear Optics Property and Type I Phase Matchability. In both compounds, the niobium oxide-fluoride BBUs exist in centric environments. In (**I**) the $[NbOF_5]^{2-}$ exists as a centric, disordered anion; in (**II**) the 1D BBUs of $[NbO_{2/2}F_4]^-$ are aligned antiparallel with respect to each other. The remaining components of the structure, polar $[Hdpa]^+$ cations, are responsible for the acentric space groups and resulting NLO responses. Polar Λ-shaped BBUs have been previously used to generate acentric and PM materials.[19,49] In (**I**) and (**II**), the amine-bridged $[Hdpa]^+$ cations form Λ-shaped BBUs. In (**I**), all dpa ligands are planar and aligned along one direction (see Figure 2), and in (**II**) the polar components of the dpa ligands are aligned in the *ac* plane. The polar amines of (**II**) are along two directions with an angle of 17.5° in two planes with an angle of 62.7° (see Figure 3). The SHG responses of the polar lambda(Λ)-shaped dpa molecules in (**I**) and (**II**) originate from donor (−NH−)/acceptor (−CN−) intramolecular interactions via π-conjugated system in acentric space group *P*1 or *Cc*. The amine donor shows a dipole moment change with the acceptor. On a molecular scale, the extent of charge transfer across the NLO chromophore determines the level of SHG output; the larger SHG output results from the greater charge transfer. In most of delocalized aromatic π electron systems, the charge transfer (CT) contribution to the second-order NLO hyperpolarizability (β) is unidimensional. In these polar Λ-shaped dpa molecules, two independent donor−acceptor moieties are linked in such a way that the charge transfer from donor group to both acceptor groups has a two-dimensional character. This can avoid charge compensation and enhance the value of β. The dpa molecules are arranged as parallel arrays in both structures of (**I**) and (**II**) (Figure 2 and Figure 3, respectively) with dpa π stacking; the aromatic molecules are separated by distances planes of 3.5960(2) Å for (**I**) and 3.9804(1) Å for (**II**). The extent of charge transfer and intermolecular interactions arrive from the delocalized π electrons that can generate large SHG response.

Although (**I**) and (**II**) are both SHG active (Figure 6), (**I**) is non-PM and (**II**) is PM. Crystallization within an NCS space group is not sufficient for a material to display useful NLO properties. A crystal which exhibits phase matching requires a large birefringence and low dispersion. The phase matching angle about the optic axis of the crystal can be calculated or measured experimentally.[12,13] It is extremely sensitive to the refractive index of the material. Refractive indices of crystals are related to the charge transfer (CT) and polarizability tensor of the structure.[70−72] Thus, the phase matchability of an NCS material is intrinsic to its crystal structure. The relationships between microscopic and macroscopic optical nonlinearities of molecular crystals and the optimal orientation of molecules within crystals for bulk phase matching were reported by Zyss and Oudar.[17] For NCS structures, the optimal phase matching and maximum of nonlinear coefficients are achieved when molecules align in a particular orientation (when the angle θ between the molecule charge transfer axis and the crystal optic axis has an optimal value, dependent on its particular Laue group). For Laue group 1, the optimal angle θ is 35.3°; for Laue groups *m* and 2, the optimal angle θ is 54.7°.[17−19,73] For Laue group *m*, the optimal orientation of molecules for phase matchability is achieved when the angle between the two equivalent molecular planes is $180° - 2\theta = 70.6°$.[17] For example, phase matchable 2-(*N*-prolinol)-5-nitropyridine (PNP) with angle θ of 59.6° and *N*,*N*′-bis-(*p*-nitrophenyl)-methanediamine (*p*-NMDA) with angle θ of 60.0° have been reported.[18,19] Previous reports on phase matchability have discussed individual molecular orientations within PM structures without comparison with a related non-PM phase. In the structure of (**II**), the angle between the two equivalent molecular planes is 62.7°, and the angle θ is 58.6°, which is close to the optimal value of 54.7°. Thus, (**II**) exhibits phase matching in the SHG measurement as shown in Figure 6b. For the structure of (**I**) in *P*1 space group, there is no symmetry constraint acting on the orientation of the principal dielectric axis. The angle θ was determined to be about 50.1°, which significantly deviates from the optimal value 35.3°. Thus, as shown in Figure 6a, (**I**) is non-PM. Comparison of the molecular geometry of non-PM (**I**) and PM (**II**), structures with chemically similar dpa cations and niobium oxide-fluoride anions, demonstrates that the arrangement of the dpa molecules controls whether the hybrid material is PM or non-PM. That is, specific molecular arrangements can optimize phase matchability and nonlinear coefficients.[17]

■ CONCLUSION

Two new inorganic/organic hybrid NCS structures have been synthesized in $NbO_{2.5}$/dpa/HF composition space diagram with combination of direct reactants of an acentric dpa molecule and an acentric d^0 transition metal oxide Nb_2O_5 to investigate phase matchability of NCS structures. The mole

dx.doi.org/10.1021/ja4050604 | J. Am. Chem. Soc. 2013, 135, 11942−11950

ratio of dpa:Nb plays a vital role to control the formation of niobium oxide-fluoride species. When the dpa:Nb mole ratio was greater than 2:1, [the $NbOF_5]^{2-}$ anions form in the structure of the non-PM phase (**I**) $[Hdpa]_2NbOF_5{\cdot}2H_2O$, while for a dpa:Nb mole ratio <2:1, infinite chains of $[NbOF_4]^-$ anions form in the structure of the PM phase (**II**) $HdpaNbOF_4$. Specific arrangements of the organic molecules within the NCS hybrid materials were shown to optimize phase matchability and nonlinear coefficients as confirmed by our analysis and SHG measurements. Future work will investigate these effects in other hybrid and inorganic systems.

■ ASSOCIATED CONTENT

Supporting Information

Listings of crystallographic data, piezoelectric and TGA measurements for compounds (**I**) and (**II**). This material is available free of charge via the Internet at http://pubs.acs.org.

■ AUTHOR INFORMATION

Corresponding Author

krp@northwestern.edu

Notes

The authors declare no competing financial interest.

■ ACKNOWLEDGMENTS

This work was supported by funding from the National Science Foundation (Award No. DMR-1005827) and a scholarship from the China Scholarship Council (H.L.). The single-crystal X-ray data and FTIR measurements were acquired at Northwestern University's Integrated Molecular Structure Education and Research Center (IMSERC) at Northwestern University which is supported by grants from NSF-NSEC, NSF-MRSEC, the KECK Foundation, the State of Illinois, and Northwestern University. We additionally thank Professor Mark Ratner, Dr. Amy Sarjeant, and Charlotte Stern for helpful discussions on data acquisition and chemical structure. This work made use of the J.B.Cohen X-ray Diffraction Facility supported by the MRSEC program of the National Science Foundation (DMR-1121262) at the Materials Research Center of Northwestern University. P.S.H. and T.T.T. thank the Welch Foundation (Grant E-1457) for support. B.W.E. and J.C.N. gratefully acknowledge the support of the National Science Foundation (DMR-1207293).

■ REFERENCES

(1) Stiegman, A. E.; Graham, E.; Perry, K. J.; Khundkar, L. R.; Cheng, L. T.; Perry, J. W. *J. Am. Chem. Soc.* **1991**, *113*, 7658.
(2) Kay, H. F.; Wellard, H. J.; Vousden, P. *Nature* **1949**, *163*, 636.
(3) Stucky, G. D.; Phillips, M. L. F.; Gier, T. E. *Chem. Mater.* **1989**, *1*, 492.
(4) Hagerman, M. E.; Poeppelmeier, K. R. *Chem. Mater.* **1995**, *7*, 602.
(5) Jailaubekov, A. E.; Willard, A. P.; Tritsch, J. R.; Chan, W.-L.; Sai, N.; Gearba, R.; Kaake, L. G.; Williams, K. J.; Leung, K.; Rossky, P. J.; Zhu, X. Y. *Nat. Mater.* **2013**, *12*, 66.
(6) Ye, N.; Chen, Q.; Wu, B.; Chen, C. *J. Appl. Phys.* **1998**, *84*, 555.
(7) Nalwa, H. S. *Appl. Organomet. Chem.* **1991**, *5*, 349.
(8) Natarajan, S.; Umamaheswaran, M.; Kalyana Sundar, J.; Suresh, J.; Martin Britto Dhas, S. A. *Spectrochim. Acta, Part A* **2010**, *77*, 160.
(9) Oudar, J. L. *J. Chem. Phys.* **1977**, *67*, 446.
(10) Giordmaine, J. A. *Phys. Rev. Lett.* **1962**, *8*, 19.
(11) Smith, A. W. *Appl. Opt.* **1964**, *3*, 147.
(12) Midwinter, J. E.; Warner, J. *Br. J. Appl. Phys.* **1965**, *16*, 1135.
(13) Hobden, M. V. *J. Appl. Phys.* **1967**, *38*, 4365.
(14) Franken, P. A.; Ward, J. F. *Rev. Mod. Phys.* **1963**, *35*, 23.
(15) Mei, D.; Yin, W.; Feng, K.; Lin, Z.; Bai, L.; Yao, J.; Wu, Y. *Inorg. Chem.* **2011**, *51*, 1035.
(16) Badikov, V.; Badikov, D.; Shevyrdyaeva, G.; Tyazhev, A.; Marchev, G.; Panyutin, V.; Petrov, V.; Kwasniewski, A. *Phys. Status Solidi RRL* **2011**, *5*, 31.
(17) Zyss, J.; Oudar, J. L. *Phys. Rev. A* **1982**, *26*, 2028.
(18) Twieg, R. J.; Dirk, C. W. *J. Chem. Phys.* **1986**, *85*, 3537.
(19) Yamamoto, H.; Katogi, S.; Watanabe, T.; Sato, H.; Miyata, S.; Hosomi, T. *Appl. Phys. Lett.* **1992**, *60*, 935.
(20) Cole, J. M.; Howard, J. A. K.; MacBride, J. A. H. *Acta Crystallogr., Sect. C* **1997**, *53*, 1331.
(21) Peters, D.; Miethchen, R. *J. Fluorine Chem.* **1996**, *79*, 161.
(22) Segal, E. B. *Chem. Health Saf.* **2000**, *7*, 18.
(23) Bertolini, J. C. *J. Emerg. Med.* **1992**, *10*, 163.
(24) Halasyamani, P.; Willis, M. J.; Stern, C. L.; Lundquist, P. M.; Wong, G. K.; Poeppelmeier, K. R. *Inorg. Chem.* **1996**, *35*, 1367.
(25) In Bruker Analytical X-ray Instruments: Madison, WI, USA, 2000.
(26) Sheldrick, G. M. University of Göttingen: Germany, 2002.
(27) Altomare, A.; Burla, M. C.; Camalli, M.; Cascarano, G. L.; Giacovazzo, C.; Guagliardi, A.; Moliterni, A. G. G.; Polidori, G.; Spagna, R. *J. Appl. Crystallogr.* **1999**, *32*, 115.
(28) Burla, M. C.; Caliandro, R.; Camalli, M.; Carrozzini, B.; Cascarano, G. L.; De Caro, L.; Giacovazzo, C.; Polidori, G.; Spagna, R. *J. Appl. Crystallogr.* **2005**, *38*, 381.
(29) Sheldrick, G. *Acta Crystallogr., Sect. A* **2008**, *64*, 112.
(30) Spek, A. L. Utrecht University: Utrecht, The Netherlands, 2001.
(31) Rieckhoff, K. E.; Peticolas, W. L. *Science (New York, N.Y.)* **1965**, *147*, 610.
(32) Kurtz, S. K.; Perry, T. T. *J. Appl. Phys.* **1968**, *39*, 3798.
(33) Ok, K. M.; Chi, E. O.; Halasyamani, P. S. *Chem. Soc. Rev.* **2006**, *35*, 710.
(34) Yang, J. S., Ed. *An Introduction to the Theory of Piezoelectricity*; Springer: New York, 2005.
(35) Pearson, R. G. *Proc. Natl. Acad. Sci. U.S.A.* **1975**, *72*, 2104.
(36) Kunz, M.; Brown, I. D. *J. Solid State Chem.* **1995**, *115*, 395.
(37) Fielicke, A.; Meijer, G.; von Helden, G. *J. Am. Chem. Soc.* **2003**, *125*, 3659.
(38) Lin, H.; Maggard, P. A. *Cryst. Growth Des.* **2010**, *10*, 1323.
(39) Gautier, R.; Donakowski, M. D.; Poeppelmeier, K. R. *J. Solid State Chem.* **2012**, *195*, 132.
(40) Halasymani, P. S.; Heier, K. R.; Norquist, A. J.; Stern, C. L.; Poeppelmeier, K. R. *Inorg. Chem.* **1998**, *37*, 369.
(41) Norquist, A. J.; Welk, M. E.; Stern, C. L.; Poeppelmeier, K. R. *Chem. Mater.* **2000**, *12*, 1905.
(42) Buslaev, Y. A.; Il'in, E. G.; Kopanev, V. D.; Gavrish, O. G. *Bull Acad. Sci. Sci. USSR Div. Chem. Sci. (Engl. Transl.)* **1971**, *20*, 1055.
(43) Agulyansky, A. *Chemistry of Tantalum and Niobium Fluoride Compounds*; Elsevier: Amsterdam, Boston, 2004.
(44) Lu, H.; Gautier, R.; Li, Z.-X.; Jie, W.; Liu, Z.; Poeppelmeier, K. R. *J. Solid State Chem.* **2013**, *200*, 105.
(45) Porter, Y.; Ok, K. M.; Bhuvanesh, N. S. P.; Halasyamani, P. S. *Chem. Mater.* **2001**, *13*, 1910.
(46) Goodey, J.; Broussard, J.; Halasyamani, P. S. *Chem. Mater.* **2002**, *14*, 3174.
(47) Jerphagnon, J.; Kurtz, S. K. *Phys. Rev. B* **1970**, *1*, 1739.
(48) Metizer, A. H.; Tiersten, H. F.; Warner, A. W.; Berlincourt, D.; Couqin, G. A.; Welsh, F. S.III. *IEEE Standard on Piezoelectricity*; IEEE: New York, 1988.
(49) Donakowski, M. D.; Gautier, R.; Yeon, J.; Moore, D. T.; Nino, J. C.; Halasyamani, P. S.; Poeppelmeier, K. R. *J. Am. Chem. Soc.* **2012**, *134*, 7679.
(50) Norquist, A. J.; Heier, K. R.; Stern, C. L.; Poeppelmeier, K. R. *Inorg. Chem.* **1998**, *37*, 6495.
(51) Ilyin, E. G.; Zozulin, A. N.; Buslaev, J. A.; Kurnakov, N. S. *J. Fluorine Chem.* **1989**, *45*, 41.
(52) Kasamatsu, Y.; Toyoshima, A.; Haba, H.; Toume, H.; Tsukada, K.; Akiyama, K.; Yoshimura, T.; Nagame, Y. *J. Radioanal. Nucl. Chem.* **2009**, *279*, 371.

(53) Monroy-Guzman, F.; Trubert, D.; Brillard, L.; Hussonnois, M.; Constantinescu, O.; Naour, C. L. *J. Mex. Chem. Soc.* **2010**, *54*, 24.
(54) Il'in, E. G.; Zozulin, A. N.; Buslaev, Y. A. *Dokl. Phys. Chem.* **2002**, *384*, 109.
(55) Lusi, M.; Barbour, L. J. *Cryst. Growth Des.* **2011**, *11*, 5515.
(56) Stomberg, R.; Svensson, I.-b.; Trysberg, L. *Acta. Chem. Scand. A* **1981**, *35*, 779.
(57) Welk, M. E.; Norquist, A. J.; Arnold, F. P.; Stern, C. L.; Poeppelmeier, K. R. *Inorg. Chem.* **2002**, *41*, 5119.
(58) Feng, Y.; Meng, Z.; Huang, Q.; Qiu, D.; Shi, H. *Inorg. Chem. Commun.* **2010**, *13*, 1118.
(59) Buslaev, Y. A.; Il'in, E. G. *Akad. Nauk SSSR, Ser. Neorgan. Mat.* **1971**, *7*, 184.
(60) Niwas Singh, R.; Padma, D. K. *J. Fluorine Chem.* **1994**, *68*, 67.
(61) Pakhomov, V. I.; Kaidalova, T. A. *Kristallografiya* **1974**, *19*, 733.
(62) Zhao, Z.; Zhou, B.; Su, Z.; Zhao, J.; Li, Z. *J. Mol. Struct.* **2009**, *928*, 171.
(63) Pushilin, M. A.; Gerasimenko, A. V.; Davidovich, R. L. *Acta Crystallogr., Sect. E* **2007**, *63*, m2086.
(64) Gerasimenko, A. V.; Pushilin, M. A.; Davidovich, R. L. *Acta Crystallogr., Sect. C* **2008**, *64*, m358.
(65) Chowdhury, S.; Gou, S.; Chakraborty, P.; Naskar, J. P. *J. Ind. Chem. Soc.* **2008**, *85*, 813.
(66) Ha, K. *Z. Kristallogr. - New Cryst. Struct.* **2010**, *225*, 653.
(67) Hurley, T. J.; Robinson, M. A. *Inorg. Chem.* **1968**, *7*, 33.
(68) Gultneh, Y.; Khan, A. R.; Blaise, D.; Chaudhry, S.; Ahvazi, B.; Marvey, B. B.; Butcher, R. J. *J. Inorg. Biochem.* **1999**, *75*, 7.
(69) Albert Cotton, F.; Daniels, L. M.; Jordan, Iv, G. T.; Murillo, C. A. *Polyhedron* **1998**, *17*, 589.
(70) Pan, F.; Bailey, R. T.; Cruickshank, F. R.; Pugh, D.; Sherwood, J. N. *J. Appl. Phys.* **1996**, *80*, 4649.
(71) Miller, E. K. *J. Chem. Phys.* **1998**, *108*, 1390.
(72) Oudar, J. L.; Zyss, J. *Phys. Rev. A* **1982**, *26*, 2016.
(73) Miyata, S.; Tao, X. T. *Synth. Met.* **1996**, *81*, 99.